Research Article

Azo Dye Derivatives As Dual-Application Materials: Anti-Prostate Cancer And Nonlinear Optical Properties Investigation

Mohammed Hafedh Hameed[1]*, Adil Muala Dhumad[1]

[1]Department of Chemistry, College of Education for Pure Sciences, University of Basrah, Basrah 61001, Iraq
*Corresponding author (e-mail address: pgs2226@uobasrah.edu.iq)

Abstract

In this study, three azo dyes derived from 2-naphthol, 2-aminobenzoic acid, 3-aminobenzoic acid, and 4-aminobenzoic acid were prepared. They were designated 2A, 3A, and 4A, respectively. The prepared compounds were characterized spectroscopically using mass, FT-IR, ^{1}HNMR, and ^{13}CNMR spectroscopy. Density functional theory (DFT) calculations via B3LYP/6-311++G(d,p) provided understanding of the electronic structures. The calculated energy gaps of the 2A-4A at 3.0901, 3.3760 and 3.2524 eV, respectively, show that the ortho carboxylic substituted azo dye (2A) has lower energy gap. The potential activity of the prepared azo dyes as potential cancer inhibitors, particularly for prostate cancer, was also theoretically investigated using molecular docking against the 1GS4 protein receptor. Molecular docking simulation demonstrated good affinity of the prepared azo dyes at -8.4, -7.2 and -7.7 kcal/mol, respectively, recant was associated with four hydrogen bonds in 2A. The cytotoxicity of the prepared azo dyes was then tested using the MTT assay against human prostate cancer cell line LNCaP. The calculated IC50 values were (46.97 ± 0.02), (71.11 ± 1.15), and (64.61 ± 0.06) µg/mol for azo dyes 2A-4A, respectively after 24 h of incubation after applying the azo dyes 2A-4A. The results of molecular docking were compared with the efficacy and cytotoxicity results of the prepared compounds and showed good agreement. The nonlinear optical properties of the prepared azo dyes 2A–4A are investigated using the diffraction pattern (DPs) method with 473 nm laser beam. The nonlinear refractive index values for azo dyes 2A is found to be 3.205×10^{-7} cm²/W. These high NLRI values make azo dyes 2A promising candidates for use in optical devices.

Key words: Azo dye, Molecular docking, Prostate cancer, DFT, NLO.

Introduction

Azo dyes with (N=N) group are among the common versatile organic compounds, renowned for their diverse structural, physical, and chemical properties. In addition to their classic applications in dyes and textiles, recent studies indicate their potential as multifunctional materials in photonics and biomedicine [1-5]. Azo dye derivatives have garnered increasing attention for their ability to interact with biological systems, as well as for exhibiting unique optical and electronic behaviors [6-8]. Several studies have demonstrated the anti-inflammatory, antibacterial, anticancer and biomedical sciences efficacy of a number of azo derivatives [9-17]. Given that prostate cancer is a significant health challenge, being the most common cancer among men [18-22]. Researchers are prioritizing the improvement of existing treatments or the discovery of new therapies with enhanced efficacy and fewer side effects[23,24]. Studying the molecular structures, including those of azo-based compounds, their structural modification, and their ability to interact with target proton receptors, makes them promising candidates for anticancer agents [25-30].

The significant increase in research demonstrating the optical properties of various azo derivatives is also noteworthy[31-33]. Recent years have witnessed a qualitative leap in the application of these properties across numerous modern technological fields [34-38]. This is attributed to the growing understanding of the interaction of high-intensity light with different compounds in the fields of optical communications and information systems, where nonlinear properties form a fundamental principle in the development of devices and protocols, including the advancement of optical computing and optical signals [39-41].

Among the most important applications are ultrafast light converters, nonlinear signal amplifiers, and wavelength converters. Vital applications have also emerged in the field of biomedical imaging, particularly the second-harmonic generation microscope, an indispensable imaging tool [42-44]. This technique surpasses conventional fluorescence microscopy because it relies on the intrinsic contrast of the tissue itself without the use of external dyes, thus avoiding the problem of light fading. This makes it ideal for long-term live imaging and is used to image collagen fibers and neural tissues [45]. Azo compounds, in particular, have demonstrated the ability to form broad diffraction rings under laser influence, making them promising compounds for use in optical selectors and switches [46-48].

This dual application of azo dye derivatives, as multifunctional materials, allows for multiple uses in nonlinear optics and biological activity against cancer in general and prostate cancer in particular. This study attempts to explore the effect of the substituent position in azo dyes on the structural and electronic properties of the dye, which in turn affects its nonlinear optical properties on the one hand and its anticancer biological activity on the other. Based on theoretical and experimental convergences, this provides a clear view of the molecular structure of azo dyes and thus offers dual-application materials that contribute effectively to the development of potential cancer therapies and technologies.

EXPERIMENTAL

Materials

All reagents were of analytical grade and used without further purification. 2-, 3-, and 4-aminobenzoic acid, 2-naphthalenol, sodium hydroxide, hydrochloric acid, and ethanol were obtain from Merck. Deionized water was used throughout all synthesis.

General procedure for synthesis azo dyes 1 and 2

Diazonium salts were synthesis by dissolving 6 mmol of 2-, 3-, and 4-aminobenzoic acid (each separately) in 2.1 mL of 36%(w/w) HCl with 5 mL of deionized water, followed by cooling to 0-5 °C. A solution of sodium nitrite (0.456 g in 5 mL deionized water) was added dropwise under stirring while maintaining the temperature below 5 °C.

Separately, (6 mmol, 0.864 g) of 2-naphthalenol was dissolved in 50 mL of deionized water, and 1.8 g of NaOH in 10 mL of deionized water was added. The solution was cooled to 0-5 °C, after which the diazonium solution was introduced slowly with stirring to effect coupling. The reaction mixture was left for 24 h to complete precipitation.

The product was acidified with dilute HCl to adjust the pH to 6-7, converting the azo compound from its sodium salt to the hydrogen dye form. The precipitate was filtered, dried, and purified by recrystallization from ethanol. Figure 1. illustrates the steps involved preparing azo dyes 2A-4A.

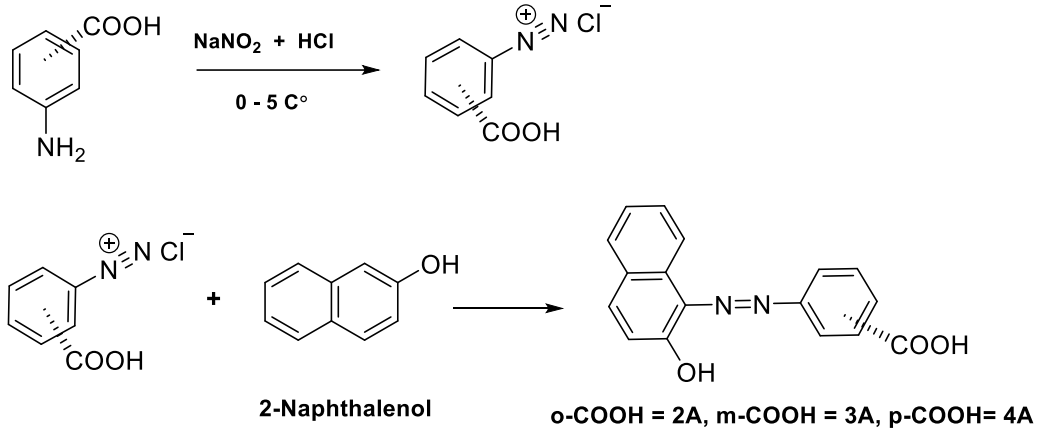

Figure 1. The steps involved preparing azo dyes 2A-4A

Synthesis of azo dye 2-((2-hydroxynaphthalen-1-yl)diazenyl)benzoic acid (2A)

The azo dye **2A** OC(C=C1)=C(N=NC2=C(C(O)=O)C=CC=C2)C3=C1C=CC=C3 was synthesized following the general procedure by reacting (6mmol, 1.7537 g) of 2-aminobenzoic acid with (6mmol, 0.8650 g) of 2-naphthalenol (Figure 1. 1).

Red solid. Yield: 73%, m.p: 286-287°C, FT-IR (KBr, cm^{-1}): C=O (1712), C=C aromatic (1600-1504), N=N (1450), C-N (1327), C–O (1255) (supplementary material: Figure S1) . ^{1}H-NMR: (400MHz-DMSO-d_6) δ 16.40 (s, 1H), 13.72 (s, 1H), 8.41 (p, 1H), 8.33 (dt, 1H), 8.03 (d, 1H), 7.91 – 7.82 (m, 1H), 7.75 (t, 1H), 7.71 – 7.63 (m, 1H), 7.62 – 7.53 (m, 1H), 7.45 (dt, 1H), 7.30 (t, 1H), 6.66 (dd, 1H), (supplementary material: Fig. S2). ^{13}C NMR (101 MHz, DMSO-d_6) δ 179.56 (C=O), 168.01 (C-O), 144.46 (C-N), 134.93, 133.73, 131.94, 130.98, 130.03, 129.71, 128.75, 127.58, 127.25, 124.91, 122.61, 117.42, and 116.72 (Ar-C) (supplementary material: Fig. S3). MS m/z for M^+ (100%) $[C_{17}H_{12}N_2O_3]^+$, 292, (supplementary material: Fig. S4).

Synthesis of azo dye 3-((2-hydroxynaphthalen-1-yl)diazenyl)benzoic acid (3A)

The azo dye **3A** OC(C=C1)=C(N=NC2=CC(C(O)=O)=CC=C2)C3=C1C=CC=C3 was synthesized following the general procedure by reacting (6mmol, 1.7537 g) of 2-aminobenzoic acid with (6mmol, 0.8650 g) of 2-naphthalenol (Fig. 1).

Red solid. Yield: 66%, m.p: 242-245°C, FT-IR (KBr, cm^{-1}): C–H aromatic (3055), C=O (1693), C=C aromatic (1618 -1504) N=N (1448), C-N (1298), C–O (1251), (supplementary material: Fig. S5). ^{1}H-NMR: (400MHz-DMSO-d_6) 15.65 (s, 2H), 13.30 (s, 2H), 8.47 (d, 2H), 8.30 (s, 2H), 8.10 – 8.02 (m, 2H), 7.94 (dd, 2H), 7.90 (d, 2H), 7.77 (d, 2H), 7.64 (q, 4H), 7.46 (t, 2H), 6.89 (dd, 2H). (supplementary material: Fig. S6). ^{13}C NMR (101 MHz, DMSO-d_6) δ 170.60 (C=O), 167.21 (C-O), 145.56 (C-N), 133.13, 132.90, 130.59, 129.92, 129.74, 129.47, 128.59, 128.39, 126.59, 124.62, 123.32, 121.72, and 119.45 (Ar-C) (supplementary material: Fig. S7). MS m/z for $C_{16}H_{11}N_3O_3$: 293 [M^+] (supplementary material: Fig. S8).

Synthesis of azo dye 4-((2-hydroxynaphthalen-1-yl)diazenyl)benzoic acid (4A)

The azo dye **3** OC(C=C1)=C(N=NC2=CC=C(C(O)=O)C=C2)C3=C1C=CC=C3was synthesized following the general procedure by reacting (6mmol, 0.8287 g) of 4-nitroaniline with (6mmol, 0.8650 g) of 2-naphthalenol (Fig. 1).

Red solid. Yield: 71%, m.p: 264-266°C, FT-IR (KBr, cm^{-1}): C=O (1678), C=C aromatic (1622–1500) N=N (1427), C-N (1290), C–O (1259), (supplementary material: Fig. S9). ^{1}H-NMR: (400MHz-DMSO-d_6) 15.88 (s, 1H), 13.01 (s, 1H), 8.44 (t, 1H), 8.05 (d, 2H), 7.93 (dd, 1H), 7.89 – 7.82 (m, 2H), 7.73 (d, 1H), 7.60 (t, 1H), 7.47 (t, 1H), 6.78 (dd, 1H). (supplementary material: Fig. S10). ^{13}C NMR (101 MHz, DMSO-d_6) δ 176.54 (C=O), 167.22 (C-O), 147.04 (C-N), 133.18, 131.57, 130.63, 130.05, 129.70, 128.55, 127.33, 126.03, 122.23, and 117.81 (Ar-C) (supplementary material: Fig. S11). MS m/z for $C_{16}H_{11}N_3O_3$: 293 [M^+] (supplementary material: Fig. S12).

RESULTS AND DISCUSSION

Chemistry

Diazoteation and coupling reactions yielded good azo dye derivatives, exhibiting intense coloring due to the extended π conjugation across the aromatic rings and the azo group. Spectral characteristics confirmed the success of the synthesis: FTIR spectra showed characteristic stretching vibrations of the –N=N– groups, along with characteristic peaks for the COOH and hydroxyl groups. ^{1}H NMR and ^{13}C NMR spectra further supported the structural determinations, showing chemical shifts consistent with protons and aromatic carbons, as well as low-field signals indicating the presence of electron-withdrawing nitro substituents.

Computational chemistry details

Density functional theory (DFT) calculations were carried at the B3LYP/6-311++G(d,p). DFT calculations indicated a decrease in the energy gap between the highest occupied molecular orbital (HOMO) and the lowest unoccupied molecular orbital (LUMO) upon substitution of the carboxyl group, which facilitates charge transfer within the conjugated system. The lowest energy gap (Egap) is found in azo dyes 2A (3.0906 eV), while it is found in azo dyes 3A and 4A (3.376 and 3.252 eV, respectively). This substitution stabilizes the lower unoccupied molecular orbital (LUMO) while slightly destabilizing the higher occupied molecular orbital (HOMO), thereby narrowing the energy gap and shifting the absorption band towards longer wavelengths. These spectral modifications are consistent with classical substitution effects in azo chromophores, where the contributions of resonance and induction together determine the optical response. Figure 2 shows the visual representation of the molecular orbitals (MO) and Egap of the prepared azo dyes.

The carboxyl group (COOH) has a weaker inductive and resonant repulsive effect. It significantly increases the azo bond length at the ortho position of azo dye 2A (1.27240 Å) due to hydrogen bond formation. At the meta position of azo dye 3A (1.26159 Å) and the para position of azo dye 4A (1.25909 Å). The dipole moment of prepared azo dyes is highest at the ortho position of azo dye 2A (4.8620 D), followed by the para position of azo dye 4A (4.7966 D), and lowest at the meta position of azo dye 3A (2.4649 D). This is because the carboxyl group at the ortho and bar positions has two effects: inductive and resonant, while at the meta position it has only one effect: inductive. Polarization(α) and hyperpolarization (β) values (17.60 x 10^{-24}, 17.41 x 10^{-24}, and 17.38 x 10^{-24}esu) and (140.68 x 10^{-32}, 69.56 x 10^{-32}, and 71.98 x 10^{-32}esu) , respectively. These values were compared with the values of urea, which serve as a common reference for this study[49]. The values for urea were 3.44 x 10^{-24} and 12.22 x 10^{-32}, respectively.

The calculations show that the polarizability and hyperpolarization of the prepared azo dyes are higher than of urea, with dye 2A exhibiting the highest values, 5 and 7 times higher than urea. These results indicate that azo dye 2A is a promising candidate material with nonlinear optical properties. Table 1 lists the calculated values of the prepared azo dyes for the MO energies, Egap, μ, α, and β.

Table 1. Calculated HOMO, LUMO, ΔEgap, μ, α, and β of prepared azo dyes 2A-4A

Comp.	HOMO (eV)	LUMO (eV)	ΔEgap (eV)	μ (Debye)	α x10^{-24} (esu)	β x10^{-32} (esu)
2A	-6.0670	-2.9764	3.0906	4.8620	17.60	140.68
3A	-5.8760	-2.5001	3.3760	2.4649	17.41	69.56
4A	-5.6624	-2.4100	3.2524	4.7966	17.38	71.98
Urea	-7.3782	-0.6764	6.7018	3.8810	3.44	12.22

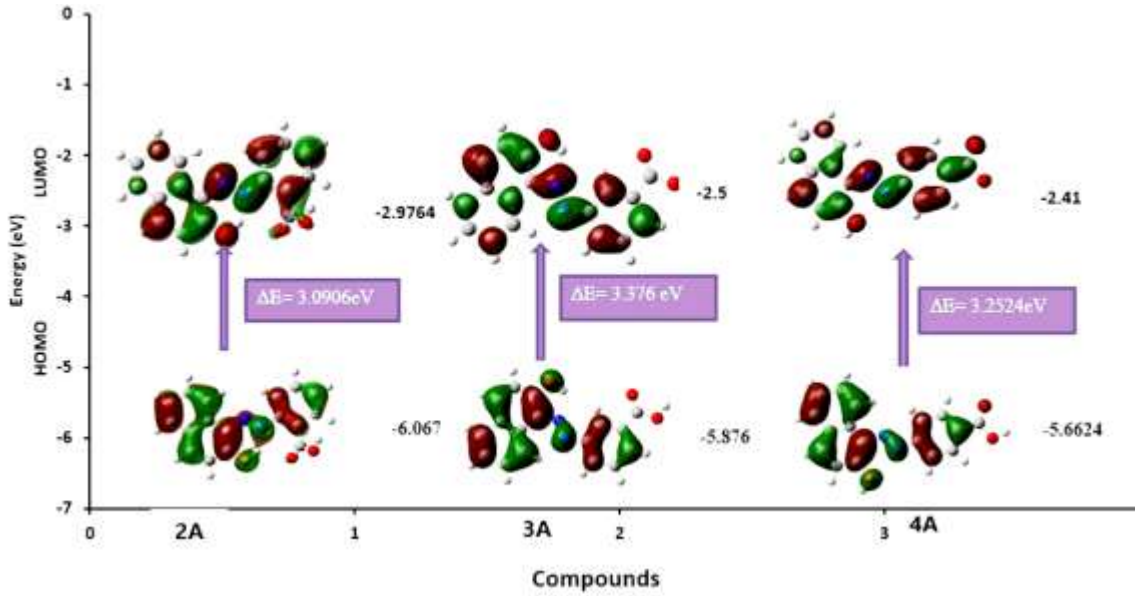

Figure 2. The HOMO, LUMO and Egap of the prepared azo dyes 2A-4A.

The electrostatic surface potential (ESP) map, shown in Figure 3 the electrical charge distribution map on the molecule's surface. The ESP highlighted the role of COOH substituents in modulating electronic transitions, thereby enhancing the chromophore properties of the dyes. Figure 3 shows the visual representation of the electron density distribution of the prepared azo dyes. The electron density (in red) distribution of the azo dye substituted with a COOH group 2A is greater across the aromatic ring double bond and the COOH group.

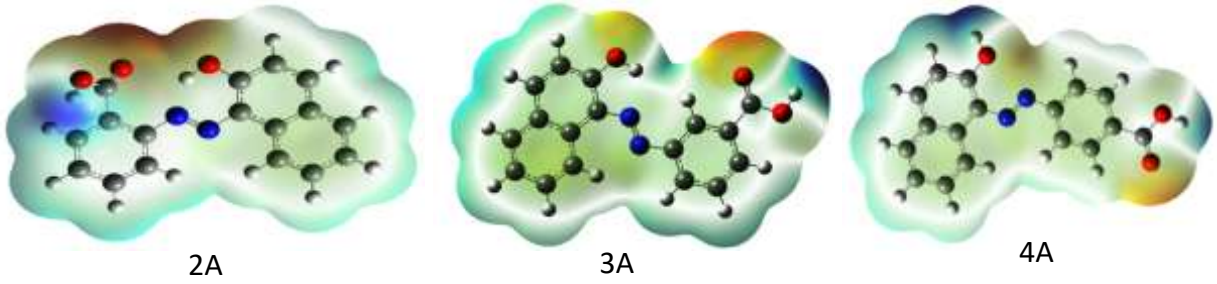

Figure 3. The electrostatic surface potential (ESP) map of the prepared azo dyes 2A-4A

Molecular docking studies

Molecular docking (MD) simulation were performed to investigation potential biological significance, specially anticancer activity[50]. The molecular docking simulation were performed of the prepared azo dyes with COOH-substituted against the (PDB ID: 1GS4). The 1GS4 is the androgen receptor, and it's primary cancer association

is prostate cancer, where it plays a key role in disease progression and treatment strategies. Before performing molecular docking simulations for the azo dyes with the receptor (PDB ID: 1GS4), the structure was proved using the Ramachandran plot diagram (Figure 4). The stereo-chemical point of the androgen receptor (PDB ID: 1GS4) was estimated using a Ramachandran diagram, which maps the backbone torsional angles (ϕ and ψ)of all non-glycine, non-proline residues. The result analysis indicated that more than 90% of amino acids residues resided the favoured place, appeared to canonical α-helix (ϕ ≈ -60°, ψ ≈ -45°) and β-sheet (ϕ ≈ -120°, ψ ≈ +120°) alteration. A few fraction of amino acid residues were located in additional allowed position, while only petty number show in disallowed position. This distribution proved the stereochemical plausibility of the receptor (PDB ID: 1GS4) template and show that the protein fold is consistent with the limitations of established structure.

Molecular docking calculations were performed for the prepared azo dyes with the receptor (PDB ID: 1GS4). As a first step, the molecular docking of the receptor was repeated with the alpha-fluorocortisol ligand already bound to it, which was downloaded from the Protein Data Bank (PDB) dedicated to receptor uploads, in order to determine the active sites and appropriate dimensions for ligand localization within the protein. The results show that the prepared azo dyes exhibited good activity, with binding energies (affinity) ranging from -7.2 kcal/mol for azo dye 3A to -8.4 kcal/mol for azo dye 2A, while the binding energy with the alpha-fluorocortisol ligand was -7.4 kcal/mol. The value of the RMSD were within accepted limits (<2.0 Å), confidence the precision of the docking simulation and supported in the binding.

The prepared azo dyes 2A-4A exhibited various interactions with amino acids at the active sites of the target receptor. Hydrogen bonding (HB) between amino acids (AA) and the active sites of the receptor ranged from two hydrogen bonds HBs formed between the target receptor 1GS4 and azo dyes 3A and 4A, to four HBs formed between the target receptor and azo dye 2A. Table 2 shows the results of MD of the prepared azo dyes with the receptor (PDB ID: 1GS4). Figure 5 show the HB visual representation of the interactions between the prepared azo dye 2A with the target receptor (PDB ID: 1GS4). Figure 6 show the two-dimensional (2D) and three-dimensional (3D) visual representation of the interactions each prepared azo dyes 2A-4A against the target receptor (PDB ID: 1GS4). These results offer that the prepared azo dye 2A could be used as models for further drug design investigations as anti-prostate cancer.

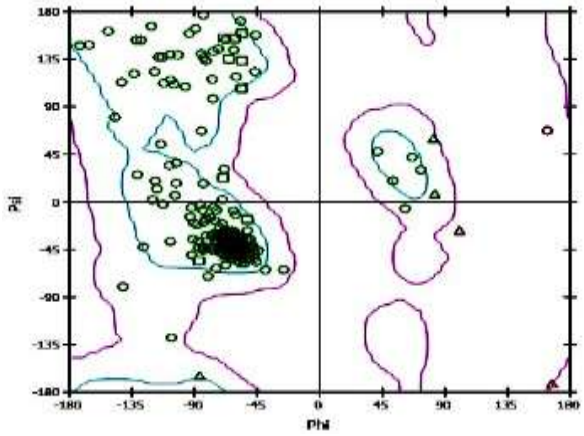

Figure 4. The Ramachandran plot of receptor (PDB ID:1GS4).

Table 2. Docking results for the prepared azo dyes with the target receptor

Comp.	affinity kcal/mol	RMSD	Interactions				
			HB	AA reside	Distance Å	Hydrophobic	Electrostatic
2A	-8.4	1.94	4	Val684 Val685 Gln711 Arg752	2.22 2.96 3.64 3.08	9	2 (π-anion)
3A	-7.2	2.04	2	Gln711 Gly683	2.77 2.91	5	1 (π-anion)

4A	-7.7	2.16	2	Arg752 Gly683	2.61 2.46	15	1
alpha-fluorocortisol	-7.4	1.98	3	His701 Gin711 Arg752	3.88 3.18 3.77	4	-

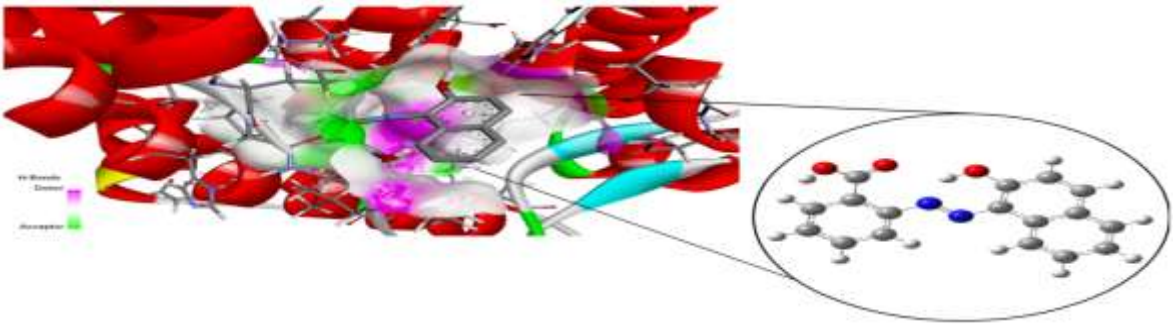

Figure 5. The HB visual representation of the interactions between the prepared azo dye 2A with the target receptor (PDB ID:1GS4).

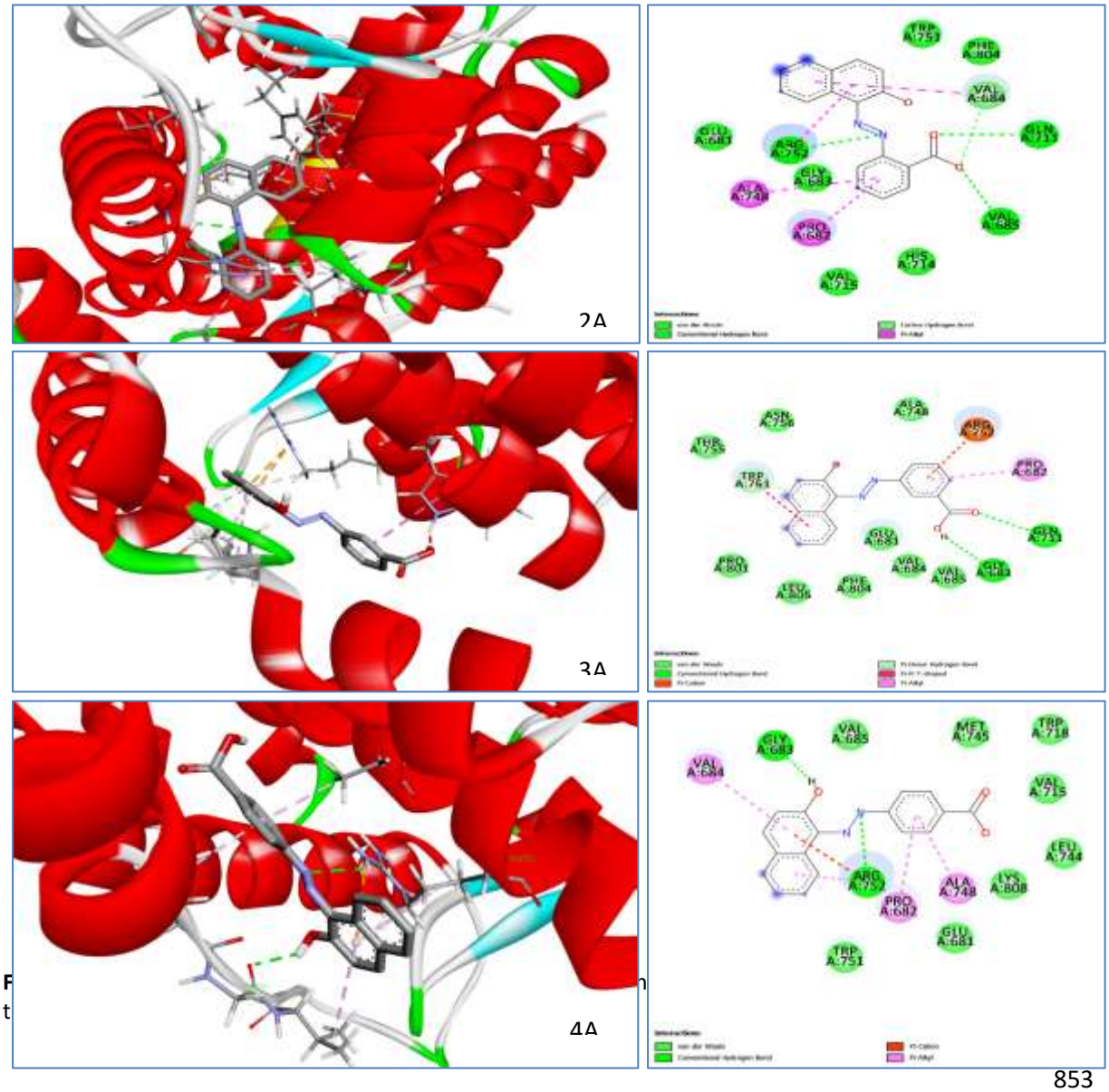

In Vitro Cytotoxicity Assay

The cytotoxicity of prepared azo dyes 2A-4A was tested, and their ability to inhibit the growth of LNCaP prostate cancer cells was evaluated using the in vitro MTT method. Different concentrations (500, 250, 125, 62.5, 31.25, and 15.62) were prepared to determine the IC_{50}. The calculated IC50 values were (46.97 ± 0.02), (71.11 ± 1.15), and (64.61 ± 0.06) µg/mol for azo dyes 2A-4A, respectively after 24 h of incubation after applying the azo dyes 2A-4A. Values are performed as means ± SE from three independent measurements at least. Figure 7 shows the relationship between concentration and of the azo dyes 2A-4A with viability of LNCaP prostate cancer cells.

Figure 7. The relationship between concentration and of the azo dyes 2A-4A with viability of LNCaP prostate

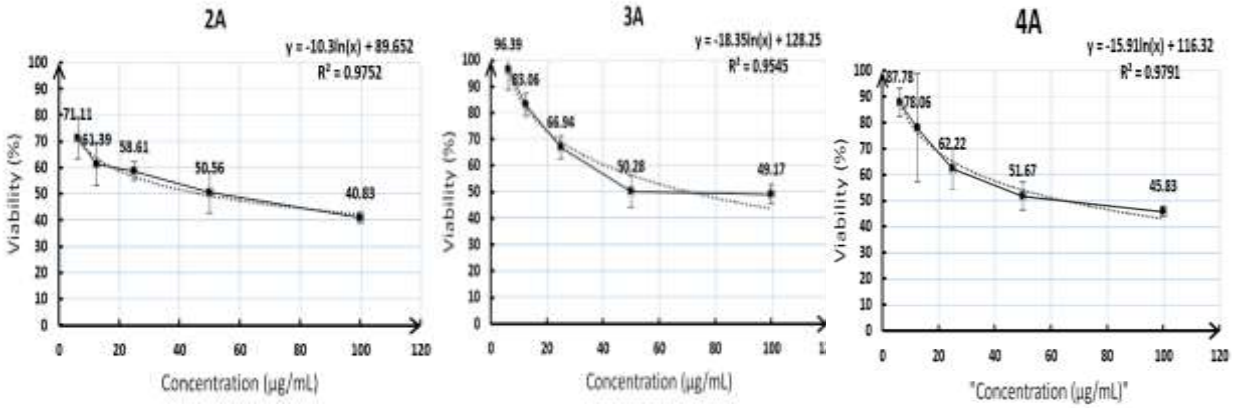

cancer cells.

Optical Properties

The optoelectronic properties of the prepared azo dye 2A were studied using the diffraction ring (DR) technique, in which the NL refractive index is calculated by counting the number of DRs visible on a screen using a 1 mm thick glass cell. The experimental results obtained from the diffraction rings were compared with theoretical results using a theoretical solution of the Fresnel-Kirchoff diffraction model. A reasonable agreement was found with the experimental results for the studied compound[51].

To obtain the DRs, a solid-state laser emitting a continuous-wavelength (CW) laser beam with a diameter of 1.5 mm (at e^{-2}) was used. The distance between the laser output coupler and the 1 mm thick glass sample cell was 40 cm. The sample cell was fixed at the focal point of a positive glass lens with a focal length of 5 cm, where the beam spot diameter at the entrance of the sample cell was ω = 19.235 µm. At λ = 473 nm, the Rayleigh length, Z_R, is 2.46 mm, making the thin-sample standard valid.

Diffraction Ring Patterns

Figure 8 shows the DR patterns produced by a 19.235 µm laser beam with a Gaussian intensity distribution as the input power is gradually increased from 0 mW to 60 mW in the solution of azo dye 2A. It is observed that as the laser input power increases, the ring patterns undergo significant changes. The upper half of the ring patterns loses symmetry; that is, it compresses and grows at a lower rate compared to the lower half and the horizontal segments. This behavior is attributed to an increase in the vertical convection current, resulting from the increased energy absorbed by the 3N compound solution, which in turn leads to a localized increase in the solution's temperature.

This temperature increase leads to a rise in the refractive index the solution of azo dye 2A, which in turn causes phase changes in the laser beam. Each outer ring in every mode is denser than the inner rings due to the self-scattering phenomenon resulting from the Gaussian distribution of the continuous laser beam. The density of the medium along the laser beam axis reaches its maximum value, making the optical path length shorter than near the edges of the Gaussian laser beam—a phenomenon known as negative thermal lensing. The number of rings and the area of each mode also increase with increasing input power.

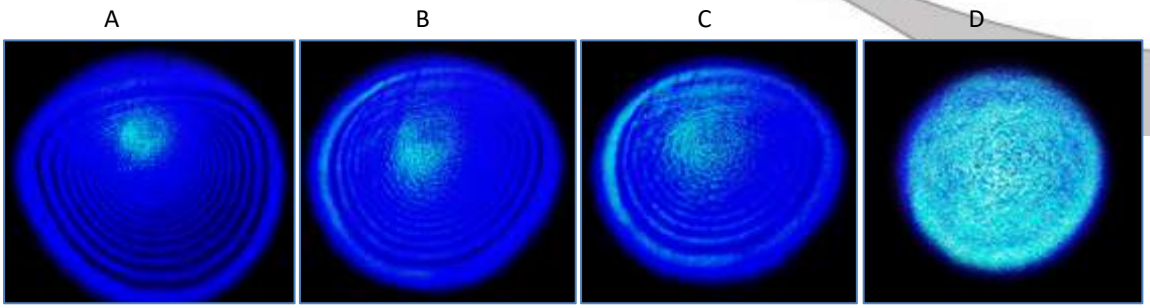

Figure 8. Input power effect on DR patterns in a solution of azo dye 2A in (mW): (a) 12, (b) 32, (c) 46, and (d) 60.

Determination of the Nonlinear Refractive Index

One ring appears when the phase of the laser beam changes by 2π radians. For N rings, the total phase change of the laser beam, Δϕ, is 2Nπ radians, which can be related to the wavelength of the radiation, λ, the thickness of the sample, d, and the total change in the refractive index of the medium, Δn, as follows:

$$\Delta\varphi = \frac{2\pi}{\lambda} d\Delta n$$

Therefore, the nonlinear refractive index, n_2, can be determined using formula [52].

$$n_2 = \frac{\pi\omega^2}{2P}\frac{N\lambda}{d}$$

At ω = 19.235 μm, N = 7, λ = 473 nm, P = 60 mW, then

$n_2 = 3.205 \times 10^{-7}$ cm²/W

The calculated NL refractive index of the azo dye 2A was compared with standard materials that have high NL refractive indices [53]. The NL refractive index of the solution of azo dye 2A was found to be greater than that of the materials mentioned in the references [53,54], indicating that the azo dye 2A solution is a potential candidate for use in optical devices.

Conclusion

Azo dyes were prepared with a carboxyl substituent on (ortho, meta, and para) positions using the diazotation reaction, followed by coupling reaction, in good yield. Theoretical calculations were carried out via DFT/B3LYP 6-311++ G(d,p), to investigate molecular structure, electronic and optical properties. The prepared azo dye 2A indicated the nonlinear optical properties, with their lower energy gap at 3.0906 eV, compared to the other azo dyes and urea. The molecular docking simulation were performed of the prepared azo dyes with COOH-substituted against the (PDB ID: 1GS4). The results show that the prepared azo dyes exhibited good activity, with binding energies (affinity) ranging from -7.2 kcal/mol for azo dye 3A to -8.4 kcal/mol for azo dye 2A, while the binding energy with the alpha-fluorocortisol ligand was -7.4 kcal/mol. The value of the RMSD were within accepted limits (<2.0 Å). The cytotoxicity of prepared azo dyes 2A-4A was tested, and their ability to inhibit the growth of LNCaP prostate cancer cells was evaluated using the in vitro MTT method. Different concentrations (500, 250, 125, 62.5, 31.25, and 15.62) were prepared to determine the IC50. The calculated IC50 values were (46.97 ± 0.02), (71.11 ± 1.15), and (64.61 ± 0.06) μg/mol for azo dyes 2A-4A, respectively. The diffraction pattern (DPs) method was used to investigate the NLO properties of azo dyes 2A-4A. The nonlinear refractive index values for azo dyes 2A is found to be 3.205×10^{-7} cm²/W. These high NLRI values make azo dyes 2A promising candidates for use in optical devices. Based on theoretical calculations, molecular docking results, cytotoxicity, relatively low IC_{50} to azo dye 2A, as well as its NLO properties, azo dye 2A considered a promising candidate for dual medical applications as an anti-prostate cancer agent and nonlinear optical activity.

References

[1] Nurul Asma Razali, Zuhair Jamain, Synthesis, chemical identification and biological application of Azo-based molecules containing different terminal group: A review, Journal of Molecular Structure, 1284, 2023,135329. https://doi.org/10.1016/j.molstruc.2023.135329.

[2] Chung, K. T. (2016). Azo dyes and human health: A review. Journal of Environmental Science and Health, Part C, 34(4), 233-261. https://doi.org/10.1080/10590501.2016.1236602

[3] Tahir T, Ashfaq M, Asghar H, Shahzad MI, Tabassum R, Ashfaq A. Medicinal Importance of Azo and Hippuric Acid Derivatives. Mini Rev Med Chem. 2019;19(9):708-719.
https://doi:10.2174/1389557518666180727162018.
[4] Ghasemi, Z., Azizi, S., Salehi, R. et al. Synthesis of azo dyes possessing N-heterocycles and evaluation of their anticancer and antibacterial properties. Monatsh Chem 149, 149–157 (2018).
https://doi.org/10.1007/s00706-017-2073-y
[5] Moustafa A. Gouda, Hadeer Fakhr Eldien, Margret M. Girges, Moged A. Berghot, Synthesis and antitumor evaluation of thiophene based azo dyes incorporating pyrazolone moiety, Journal of Saudi Chemical Society, 20, Issue 2, 2016, Pages 151-157. https://doi.org/10.1016/j.jscs.2012.06.004.
[6] Jerca, F.A., Jerca, V.V. & Hoogenboom, R. Advances and opportunities in the exciting world of azobenzenes. Nat Rev Chem 6, 51–69 (2022). https://doi.org/10.1038/s41570-021-00334-w
[7] unjie Ding, Ze Huang, Duoteng Zhang, Yunwei Qu, Shiji Zhang, Congcong Zhang, Bin Fang, Lin Li, Wei Huang; Rational structural design of aromatic Azo photoactive small molecules for biomedical applications. Chem. Soc. Rev. 2025; 54 (22): 10363–10396. https://doi.org/10.1039/d5cs00334b
[8] V. Y. Chang, C. Fedele, A. Priimagi, A. Shishido, C. J. Barrett, Photoreversible Soft Azo Dye Materials: Toward Optical Control of Bio-Interfaces. Advanced Optical Materials 2019, 7, 1900091.
https://doi.org/10.1002/adom.201900091
[9] Elgammal, W. E., Ali, A. A., Elhagali, G. A., Ismail, M. A., Belal, A., Albezrah, N. K., ... & El-Gaby, M. S. (2025). Innovative azo disperse dyes containing a hydrazide–hydrazone moiety: design, DFT calculations, antimicrobial and antibiofilm activities, and dyeing performance on polyester fabrics. ACS omega, 10(35), 39567-39579.
https://doi.org/10.1021/acsomega.5c02445
[10] Hsuan-Ping Chang, Se Jin Kim, Dhaval K. Shah, Whole-Body Pharmacokinetics of Antibody in Mice Determined using Enzyme-Linked Immunosorbent Assay and Derivation of Tissue Interstitial Concentrations, Journal of Pharmaceutical Sciences, 110, Issue 1, 2021, Pages 446-457.
https://doi.org/10.1016/j.xphs.2020.05.025.
[11] Yousaf Ali, Shafida A. Hamid and Umer Rashid, Nov 2018, Biomedical Applications of Aromatic Azo Compounds, Mini Reviews in Medicinal Chemistry, Volume 18, Issue 18, p. 1548 – 1558.
https://doi.org/10.2174/1389557518666180524113111.
[12] Sangar Ali Hassan, Dara Muhammed Aziz, Dana A. Kader, Hiwa Omer Ahmad, Media Noori, Alla Ahmad M. Amin, Hevin Jumha Qurbani, Shivan Mustafa Husein, Govan Hamid Hamasdiq, Synthesis and characterization of Azo-Azomethine derivatives bearing thiazole moiety: In vitro antimicrobial, in vitro and in vivo anti-inflammatory, and cytotoxicity assessment, accompanied by computational molecular docking, RDG, ELF, DFT, and MEP analysis, Journal of Molecular Structure, Volume 1318, Part 2, 2024, 139294.
https://doi.org/10.1016/j.molstruc.2024.139294.
[13] T. A.YEŞİL, New Azo-Azomethine Compounds: Comprehensive Evaluation of In Silico Biological Activities, ADMEt Profiling, and In Vitro Antioxidant Properties. ChemistrySelect2025, 10, e202405875.
https://doi.org/10.1002/slct.202405875
[14] S. Harisha, Jathi Keshavayya, S.M. Prasanna, H. Joy Hoskeri, Synthesis, characterization, pharmacological evaluation and molecular docking studies of benzothiazole azo derivatives, Journal of Molecular Structure, 1218, 2020, 128477. https://doi.org/10.1016/j.molstruc.2020.128477.
[15] Ruth Sahilu, Rajalakshmanan Eswaramoorthy, Endale Mulugeta, Aman Dekebo, Synthesis, DFT analysis, dyeing potential and evaluation of antibacterial activities of azo dye derivatives combined with in-silico molecular docking and ADMET predictions, Journal of Molecular Structure, 1265, 2022, 133279.
https://doi.org/10.1016/j.molstruc.2022.133279.
[16] Kibrom Mezgebe, Endale Mulugeta, Synthesis and pharmacological activities of azo dye derivatives incorporating heterocyclic scaffolds: a review, RSC Advances, Volume 12, Issue 40, 2022, Pages 25932-25946,
https://doi.org/10.1039/d2ra04934a.
[17] Khan, Md N., Digvijaysinh K. Parmar, and Debasis Das. "Recent applications of azo dyes: A paradigm shift from medicinal chemistry to biomedical sciences." Mini Reviews in Medicinal Chemistry 21.9 (2021): 1071-1084.
https://doi.org/10.2174/1389557520999201123210025
[18] Rawla, P. (2019). Epidemiology of prostate cancer. World journal of oncology, 10(2), 63.
https://doi:10.14740/wjon1191
[19] Ballentine Carter, H., & Coffey, D. S. (1990). The prostate: an increasing medical problem. The prostate, 16(1), 39-48. https://doi.org/10.1002/pros.2990160105

[20] Kratzer, T. B., Mazzitelli, N., Star, J., Dahut, W. L., Jemal, A., & Siegel, R. L. (2025). Prostate cancer statistics, 2025. CA: A Cancer Journal for Clinicians, 75(6), 485-497. https://doi.org/10.3322/caac.70028
[21] De Nunzio, C., Lombardo, R. Best of 2025 in prostate cancer and prostatic diseases. Prostate Cancer Prostatic Dis 29, 216–221 (2026). https://doi.org/10.1038/s41391-026-01083-x
[22] Chu, F., Chen, L., Guan, Q. et al. Global burden of prostate cancer: age-period-cohort analysis from 1990 to 2021 and projections until 2040. World J Surg Onc 23, 98 (2025). https://doi.org/10.1186/s12957-025-03733-1
[23] Hamdy, N. M., Basalious, E. B., El-Sisi, M. G., Nasr, M., Kabel, A. M., Nossier, E. S., & Abadi, A. H. (2024). Advancements in current one-size-fits-all therapies compared to future treatment innovations for better improved chemotherapeutic outcomes: a step-toward personalized medicine. Current medical research and opinion, 40(11), 1943-1961. https://doi.org/10.1038/nrd2593
[24] Rai, V., Gupta, Y., Srivastava, S. P., Shukla, A., Bano, N., & Khan, S. (2024). Targeted Therapies in Cancer Treatment: Unveiling the Latest Breakthroughs and Promising Approaches. J. Res. Appl. Sci. Biotechnol, 2, 175-183. https://doi.org/10.55544/jrasb.2.6.26
[25] De Filippis B, Della Valle A, Ammazzalorso A, Maccallini C, Tesse G, Amoroso R, Mollica A, Giampietro L. Azobenzene as Multi-Targeted Scaffold in Medicinal Chemistry. Molecules. 2024; 29(24):5872. https://doi.org/10.3390/molecules29245872
[26] Mutlu, H.; Geiselhart, C.M.; Barner-Kowollik, C. Untapped potential for debonding on demand: The wonderful world of azo-compounds. Mater. Horiz. 2018, 5, 162–183. https://doi.org/10.1039/c7mh00920h
[27] Tripathy, L., & Sarangi, A. K. (2025). Synthesis, Characterization, Biological and Computational Insights of some Binuclear Azo Dye-Based Metal Complexes. Applied Organometallic Chemistry, 39(11), e70407. https://doi.org/10.1002/aoc.70407
[28] Al-Araji, A.A., Al-adilee, K.J. Synthesis, spectroscopic characterization, and biological evaluation of novel mixed ligand bis-azo dye complexes and study antimicrobial, anticancer, and molecular docking. Discov. Chem. 3, 180 (2026). https://doi.org/10.1007/s44371-026-00636-2
[29] Afifi TH, Okasha RM, Ahmed HEA, Ilaš J, Saleh T, Abd-El-Aziz AS. Structure-activity relationships and molecular docking studies of chromene and chromene based azo chromophores: A novel series of potent antimicrobial and anticancer agents. EXCLI J. 2017 Jun 19;16:868-902. doi: 10.17179/excli2017-356.
[30] Tahir T, Ashfaq M, Saleem M, Rafiq M, Shahzad MI, Kotwica-Mojzych K, Mojzych M. Pyridine Scaffolds, Phenols and Derivatives of Azo Moiety: Current Therapeutic Perspectives. Molecules. 2021; 26(16):4872. https://doi.org/10.3390/molecules26164872
[31] Delaire, J. A., & Nakatani, K. (2000). Linear and nonlinear optical properties of photochromic molecules and materials. Chemical Reviews, 100(5), 1817-1846. https://doi.org/10.1021/cr980078m
[32] Selivanova, G.A. Azo chromophores for nonlinear-optical application. Russ Chem Bull 70, 213–238 (2021). https://doi.org/10.1007/s11172-021-3080-z
[33] Dudek, M., Kaczmarek-Kedziera, A., Deska, R., Trojnar, J., Jasik, P., Młynarz, P., Samoc, M. and Matczyszyn, K., 2022. Linear and nonlinear optical properties of azobenzene derivatives modified with an (amino) naphthalene moiety. The Journal of Physical Chemistry B, 126(32), pp.6063-6073. https://doi.org/10.1021/acs.jpcb.2c03078
[34] Kavitha, S., Saravanakumar, M., Kiranisha, A., Balasubramanian, V., Chakravarty, S., & Vijayakumar, V. N. (2025). Design, synthesis and characterisation of complementary hydrogen bond ferroelectric liquid crystals for non-linear applications: combined experimental and density functional theory approach. Liquid Crystals, 52(12), 1174–1193. https://doi.org/10.1080/02678292.2025.2594699
[35] Rezvan, V.H. DFT investigation of 5,8-diaminoquinoxaline-based alkyl bis-Schiff bases: geometry, spectroscopic analysis, MEP, frontier orbitals, and nonlinear optical characteristics. Discov. Chem. 3, 45 (2026). https://doi.org/10.1007/s44371-025-00424-4
[36] Raju, G. et al. (2025). Nonlinear Optical Microscopy for Cancer Diagnosis. In: Mazumder, N., Biswas, R., Zhuo, GY. (eds) Advanced Biophysical Techniques in Biosciences. Lecture Notes in Nanoscale Science and Technology, vol 7. Springer, Cham. https://doi.org/10.1007/978-3-031-94551-9_11
[37] Mogal Mahazira Tabassum , Yesudasu Vasimalla , Ragini Singh , Santosh Kumar , The Chemical Record 2026, 26, e202500251. https://doi.org/10.1002/tcr.202500251
[38] Bhaskar, S., Wang, W., Lee, H., Liu, L., Umrao, S., Liu, W., ... & Cunningham, B. T. (2025). Photonic crystal grating resonance and interfaces for health diagnostic technologies. Chemical reviews, 125(14), 6435-6540. https://doi.org/10.1021/acs.chemrev.4c00653
[39] Shubar MY, Saadon HL, Rahma MA. Laser-induced nonlinear far-field diffraction patterns of disperse azo dyes. Optik (Stuttg). 2025;335:172422. https://doi.org/10.1016/j.ijleo.2025.172422

[40] Hadji, D., Baroudi, B. & Bensafi, T. Nonlinear optical properties of azo sulfonamide derivatives. J Mol Model **30**, 117 (2024). https://doi.org/10.1007/s00894-024-05915-2
[41] Hu J, Song T, Yu MM, Yu H. Optically controlled solid-to-liquid phase transition materials based on azo compounds. Chemistry of Materials. 2023 Jun 12;35(12):4621-48. https://doi.org/10.1021/acs.chemmater.3c00841
[42] Bobo Gu, Chujun Zhao, Alexander Baev, Ken-Tye Yong, Shuangchun Wen, and Paras N. Prasad, "Molecular nonlinear optics: recent advances and applications," Adv. Opt. Photon. 8, 328-369 (2016). https://doi.org/10.1364/AOP.8.000328
[43] Adur J, Carvalho HF, Cesar CL, Casco VH. Nonlinear microscopy techniques: principles and biomedical applications. Microscopy and analysis. 2016 Sep 21:121-49. http://dx.doi.org/10.5772/63451
[44] Pavone FS, Campagnola PJ, editors. Second harmonic generation imaging. Boca Raton, FL, USA:: CRC Press; 2014.
[45] James R. Taylor "Tutorial on fiber-based sources for biophotonic applications," Journal of Biomedical Optics 21(6), 061010 (10 Jun 2016). https://doi.org/10.1117/1.JBO.21.6.061010
[46] Galiakhmetova, D. (2023). Development of novel compact ultrashort pulse lasers for biomedical applications (Doctoral dissertation, Aston University). https://doi.org/10.48780/publications.aston.ac.uk.00047213
[47] Mughal, E. U., Raja, Q. A., Alzahrani, A. Y. A., Naeem, N., Sadiq, A., & Bozkurt, E. (2023). Pyrimidine-based azo dyes: synthesis, photophysical investigations, solvatochromism explorations and anti-bacterial activity. Dyes and Pigments, 220, 111762. https://doi.org/10.1016/j.dyepig.2023.111762
[48] Salma Sherif, Asmaa Aboelnaga, Nagla S. Elshemy, Samia Elabbady, Sayed K. Ramadan; Design and synthesis of novel sulfa-azo dyes: a sustainable approach to textile dyeing combined with microwave energy. RSC Adv. 2026; 16 (6): 5374–5400. https://doi.org/10.1039/d5ra09499b
[49] Ravi, S., Sreedharan, R., Raghi, K. R., Manoj Kumar, T. K., & Naseema, K. (2020). Experimental and computational perspectives on linear and non-linear optical parameters of an orthorhombic crystal for optical limiting applications. Applied Physics A: Materials Science & Processing, 126(1), 1. https://doi.org/10.1007/s00339-019-3234-0
[50] Ahmed Majeed Jassem, Adil Muala Dhumad, Jinan Khudhair Salim, Hadi Abdalsamad Jabir, An alternative technique for cyclization synthesis, in vitro anti-esophageal cancer evaluation, and molecular docking of novel thiazolidin-4-one derivatives, Journal of Molecular Structure, Volume 1280, 2023,135079, https://doi.org/10.1016/j.molstruc.2023.135079.
[51] Peterzol, A., Olivo, A., Rigon, L., Pani, S. and Dreossi, D. (2005), The effects of the imaging system on the validity limits of the ray-optical approach to phase contrast imaging. Med. Phys., 32: 3617-3627. https://doi.org/10.1118/1.2126207
[52] Haleshappa D, Jayarama A, Quah CK, Kwong HC. A novel bromo-substituted thiophene based centrosymmetric crystals: Thermal, mechanical, and third order NLO properties for the optical limiting applications. Physica B Condens Matter. 2020;585:412083. https://doi.org/10.1016/j.physb.2020.412083.
[53] Maidur SR, Patil PS. Linear optical and third-order nonlinear optical properties of anthracene chalcone derivatives doped PMMA thin films. Optik (Stuttg). 2019;190:54–67. https://doi.org/10.1016/j.ijleo.2019.05.092
[54] Zaini MF, Khairul WM, Arshad S, Abdullah M, Zainuri DA, Rahamathullah R, et al. The structure-property studies and mechanism of optical limiting action of methyl 4-((4-aminophenyl) ethynyl) benzoate crystal under continuous wave laser excitation. Opt Mater (Amst). 2020;107:110087. https://doi.org/10.1016/j.optmat.2020.110087